The Pathology and Splenic Transcriptome Profiling of *Trionyx sinensis* Challenged with *Bacillus cereus*

Jinbiao Jiao [1], Jing Chen [1], Jiayun Yao [1], Yanli Li [2], Xuemei Yuan [1], Lei Huang [1], Shengqi Su [2,*] and Haiqi Zhang [1,*]

[1] Agriculture Ministry Key Laboratory of Healthy Freshwater Aquaculture, Key Laboratory of Fish Health and Nutrition of Zhejiang Province, Key Laboratory of Fishery Environment and Aquatic Product Quality and Safety of Huzhou City, Zhejiang Institute of Freshwater Fisheries, Huzhou 313001, China

[2] College of Fisheries, Key Laboratory of Freshwater Fish Reproduction and Development (Ministry of Education), Research Center of Fishery Resources and Environment, Southwest University, Chongqing 400715, China

* Correspondence: sushengqi@swu.edu.cn (S.S.); zmk407@126.com (H.Z.)

Abstract: The pathogenic *Bacillus cereus* strain XS0724 isolated from China can cause high lethality to *Trionyx sinensis*, but little information is available on their detailed interactions. In this study, histopathologic profiling indicated that *B. cereus* caused vacuolization and cell necrosis in the liver, spleen, kidney, and intestine. The identification of the virulence factor genes non-hemolytic enterotoxin (*Nhe*), hemolysin BL (*Hbl*), and enterotoxin FM (*entFM*) confirmed bacterial pathogenicity. Splenic transcriptomic sequencing at 96 h post-infection identified various immune-related genes mapped to diverse gene families, including interleukin, complement, chemokine, and interferon. The differentially expressed genes (DEGs) were enriched in 2174 GO terms: 1694 in biological processes, 138 in cellular components, and 342 in molecular functions. Further KEGG enrichment indicated that DEGs were primarily associated with the phagosome, NF-kappa B signaling pathway, and PI3K-Akt signaling pathway. The DEGs and enriched pathways may be involved in the elimination of invasive *B. cereus*. These data laid the foundation for elucidating the potential molecular mechanisms in this bacterial infection process, and provided robust genetic evidence for subsequent work on resistance genes of *T. sinensis*.

Keywords: resident bacteria; opportunistic infection; toxins; immune response; aquaculture

1. Introduction

Intensive aquaculture has recently led to bacterial diseases and huge economic losses. As key pathogens, pathogenic bacteria are rapidly spread in suitable aquatic environments, which can disrupt the normal function, metabolism, and physiology of aquatic animals by exploiting an arsenal of genes encoding virulence factors [1]. Although antibiotics and vaccines are effective in controlling distinct bacterial diseases, there exist some limitations [2]. Antibiotics risk triggering drug resistance and threatening the safety of aquatic products [3]. Despite the success of bacterial vaccines in recent years, several emerging bacterial diseases are not effectively treated by current commercially available vaccines [4]. Therefore, it is critical to elucidate the pathogenic mechanism at the molecular level for preventing pathogens and developing new strategies in the future.

Chinese soft-shelled turtle *Trionyx sinensis* is one of the main commercial freshwater-cultured species in China due to its substantial economic, nutritional, medicinal, and ornamental value. In recent years, however, with the deterioration of the water environment, increased breeding density, and degradation of germplasm resources, *T. sinensis* has suffered severe infectious diseases, including *Bacillus cereus* [5–8]. Outbreaks of these pathogens have brought severe economic losses to the aquaculture industry.

B. cereus, a Gram-positive bacteria, is regarded as a facultative anaerobe ubiquitously distributed in soil, water, sewage plants, and food [9]. It functions not only as a probiotic by reinforcing gastrointestinal balance and immune systems [10], but also as a main pathogen of food poisoning due to its virulence factors [11]. Previous studies reported that *B. cereus* caused diseases in a wide range of aquatic animal species [12,13], as well as head-shaking syndrome characterized by high mortality in *T. sinensis* [14]. These diseases have caused large economic losses to farmers. *B. cereus* group isolates carrying virulence factor genes *cytK*, *HblC*, *NheA*, and *entFM* were detected from diseased *T. sinensis* in Taiwan [8]. Whole genome sequencing of *B. cereus* strain SYJ15 from *T. sinensis* has also been reported [15]. However, little is known about the virulence factors and pathogenicity of the previous *B. cereus* strain XS0724, and this requires further study. As little is currently known about how *T. sinensis* responds to *B. cereus* strain XS0724, it is of great significance to understand the immune mechanism of *T. sinensis*.

To date, high-throughput transcriptome sequencing has been broadly applied in immune-related gene identification in many aquatic animals under bacterial challenge [16–18]. The molecular mechanism identified by RNA-seq of *T. sinensis* after *B. cereus* infection has not yet been established. Given that *B. cereus* is highly pathogenic to *T. sinensis* and molecular mechanisms of the immune response are limited, histopathological observations were carried out in this study to evaluate histopathologic changes in different organs. In addition, we utilized transcriptomic sequencing to reveal potential regulators and biological responses after pathogenic infection. These results may inform antibacterial immune activities at the transcriptional level and provide a strong theoretical basis for controlling and preventing bacterial disease in *T. sinensis*, especially against *B. cereus*.

2. Materials and Methods

2.1. Animal Infection and Sample Collection

T. sinensis individuals, each weighing 750 ± 50 g, were obtained from a commercial turtle farm (Huzhou, China). A total of 20 specific pathogen-free turtles were randomly divided into two groups: infection group (GD, n = 10) and control group (CK, n = 10). Prior to the infection experiments, the two groups were both acclimatized in a 200-L tank with aerated freshwater (28–30 °C) for one week. *B. cereus* strain XS0724 (Genebank ID: OQ255816) isolated previously [14] was freshly cultivated in tryptic soy broth (TSB) medium (Huankai Co., Ltd., Guangzhou, China) to logarithmic growth phase, and resuspended in phosphate-buffered saline (PBS) at a density of 3.84×10^6 CFU/mL. For the infection group, the turtles were injected intraperitoneally with 200 μL of fresh bacteria, while the control group was inoculated with an equal volume of PBS. At 96 h post-infection (hpi), three turtles were randomly chosen in both groups for sampling. The spleens were collected and flash frozen in liquid nitrogen for RNA extraction. Meanwhile, the livers, spleens, kidneys, and intestines from the same individuals were extracted and immersed in 4% paraformaldehyde at 4 °C for histopathologic analysis.

2.2. Histopathologic Observation

The collected livers, spleens, kidneys, and intestines (see Section 2.1) were fixed in 4% paraformaldehyde for more than 24 h. After dehydration with an ethanol gradient and embedding in paraffin, the tissues were cut into thin sections (4-μm thickness). Finally, the sections were stained with hematoxylin and eosin (HE) following standard procedures, and assessed under a microscope [19].

2.3. Detection of Virulence Factor Genes

The genomic DNA of bacteria was extracted from fresh bacterial cultures with a Bacterial Genomic DNA Extraction kit (Tiangen Biotech, Beijing, China). All PCR reactions were performed with 2 × Taq Master Mix (New England Biolabs, Ipswich, MA, USA). The reactions contained 12.5 μL of 2 × Taq Master Mix, 1 μL of template DNA, 1 μL of forward primer (10 μM), 1 μL of reverse primer (10 μM), and 9.5 μL of ddH$_2$O. The PCR

program consisted of one initial denaturation step at 95 °C for 5 min, followed by 35 cycles (denaturation at 95 °C for 30 s, annealing for 30 s, extension at 72 °C), and a final extension at 72 °C for 5 min. The PCR amplification was performed on a Bio-Rad Thermal Cycler (Bio-Rad, Hercules, CA, USA). The annealing temperature and extension time depended on the primers and target fragment lengths (about 1 min/kb), and are detailed in Table 1. PCR products were visualized by electrophoresis on a 1% agarose gel containing GelRed (Biotium, Fremont, CA, USA) to determine the presence of virulence factor genes.

Table 1. The primers used to amplify virulence factor genes.

Gene	Primer Sequence (5′ to 3′)	Product Length (bp)	Annealing (°C)	References
NheA	TACGCTAAGGAGGGGCA GTTTTATTGCTTCATCGGCT	500	55	[20]
NheB	CAAGCTCCAGTTCATGCGG GATCCCATTGTGTACCATTG	935	58	[21]
NheC	ACATCCTTTTGCAGCAGAAC CCACCAGCAATGACCATATC	618	58	[21]
NblA	GCAAAATCTATGAATGCCTA GCATCTGTTCGTAATGTTTT	884	54	[21]
HblC	CCTATCAATACTCTCGCAA TTTCCTTTGTTATACGCTGC	695	54	[21]
HblD	AATCAAGAGCTCTCACGAAT CACCAATTGACCATGCTAAT	430	52	[20]
bceT	TTACATTACCAGGACGTGCTT TGTTTGTGATTGTAATTCAGG	428	55	[22]
cytK	CGACGTCACAAGTTGTAACA CGTGTGTAAATACCCCAGTT	565	52	[21]
ces	GCATTTCGTGAAGCAGAGGT CCCTTTATCCCCTTCGATGT	699	59	[23]
entFM	GTTCGTTCAGGTGCTGGTAC AGCTGGGCCTGTACGTACTT	486	55	[21]

2.4. RNA Extraction, cDNA Library Construction, and Sequencing

The frozen spleen samples (see Section 2.1) were ground in liquid nitrogen and total RNA was extracted using RNAiso Plus Reagent (Takara, Shiga, Japan) following the manufacturer's instructions. The concentration of RNA was measured using a NanoDrop 2000 spectrophotometer (Thermo Fisher Scientific, Waltham, MA, USA) and RNA integrity was examined by an Agilent 2100 Bioanalyzer system (Agilent Technologies, Santa Clara, CA, USA).

Polyadenylated RNA was isolated from total RNA with Dynabeads Oligo (dT) (Invitrogen, Waltham, MA, USA), fragmented into 300 bp fragments, and then reverse transcribed into first strand cDNA using reverse transcriptase and random primers. The resulting suitable fragments were enriched by PCR amplification to construct the cDNA libraries. The size distribution of the cDNA libraries was validated using an Agilent Bioanalyzer 2100, and cDNA was quantified by qPCR. Sequencing of the complete libraries was performed in 150 bp paired-end mode using an Illumina HiSeq 4000 platform (Illumina, San Diego, CA, USA).

2.5. Raw Data Assembly and Annotation

Raw reads were quality controlled by clipping sequencing adapters and filtering low-quality reads (<Q20) and short reads (length < 50 bp). High-quality clean sequences were de novo assembled to obtain transcripts using Trinity 2.4.0 [24] with the default parameters. After clustering transcripts, the longest transcript was regarded as the unigene for each cluster.

All assembled unigenes were functionally annotated by aligning against public databases: NCBI non-redundant protein sequences (NR) (http://www.ncbi.nlm.nih.gov/, accessed on 17 December 2019), Swissprot (http://www.expasy.ch/sprot, accessed on 17

December 2019), Protein family (Pfam) (http://pfam.xfam.org/, accessed on 17 December 2019), Gene Ontology (GO) (http://geneontology.org/page/go-database, accessed on 17 December 2019), Kyoto Encyclopedia of Genes and Genomes (KEGG) (http://www.genome.jp/kegg, accessed on 17 December 2019), and eggNOG (http://eggnog.embl.de/, accessed on 17 December 2019) using Diamond (version 0.7.9) [25], Blast2go (version 2.5.0) [26], and KAAS (version 2.0) [27].

2.6. Identification and Patterns of DEGs

The fragments per kilobase of transcript per million mapped (FPKM) method was used to normalize and calculate gene expression. The clean read counts were obtained from the transcriptome alignment files using RSEM 1.2.12 software [28]. Differential gene expression analysis between samples was performed using the DESeq R package (1.12.0) with default parameters [29]. *p*-values were adjusted for multiple testing by the Benjamini–Hochberg procedure [30]. The threshold for defining DEGs was $|\log_2 (\text{fold change})| > 1$ and *p*-value < 0.05. Volcano and MA plots of differentially expressed genes were rendered using ggplot2 R package.

2.7. GO Term and KEGG Pathway Enrichment Analysis of DEGs

In order to clarify the biological processes and functions of DEGs, we mapped all DEGs to the GO and KEGG databases. GO functional enrichment and KEGG pathway enrichment were conducted using the topGO package and KOBAS 2.0 [31] with a threshold *p*-value < 0.05.

2.8. Analysis of Gene Expression by qPCR

To further validate the transcriptome DEG data, we selected 11 DEGs for qPCR analysis. Total RNA was extracted from frozen spleen samples as described above. RNA was reverse transcribed into cDNA using a Prime Script RT Reagent kit (Takara, Shiga, Japan). All qPCR primers were designed using Primer Premier 5.0 software (Premier Biosoft, Palo Alto, CA, USA) (Table 2). The qPCR reactions were performed with SYBR Green PCR Mastermix (Roche, Basel, Switzerland) using a Light Cycler 480 Real-Time PCR system (Roche, Basel, Switzerland), with the following parameters: 95 °C for 600 s, followed by 45 cycles (95 °C for 10 s, 60 °C for 10 s, and 72 °C for 30 s), and 95 °C for 10 s, 65 °C for 60 s and 97 °C for 1 s. All reactions, including controls, were performed in triplicate from three independently isolated RNA samples. The *β-actin* gene was utilized as an internal control for normalization [32], and the gene expression levels relative to *β-actin* gene were quantified using the comparative $2^{-\Delta\Delta CT}$ method [33]. Consistency between RNA-seq and qPCR was evaluated by linear regression analysis.

Table 2. The primers used in qPCR validation.

Primer Name	Sequence (5′ to 3′)	Product Length (bp)
DDN1-F	TAAACACAGCGGGATTCAAAC	119
DDN1-R	GGCAAACACAATGCAGAAGTA	
OCSTAMP-F	GGTGCTCCTCTCTTTGACTCTGA	85
OCSTAMP-R	CACAGCCGTGTCTGCCAAG	
TNIP1-F	TACCTTGTTCCTCATCCGCC	132
TNIP1-R	TTCAACTACCAACGCCTCCA	
IL-8-F	CGTTGGAAATGACTTAGGCAG	205
IL-8-R	TGAAACCACAAAACCCAAGTC	
CCL20-F	AACTCAGGAAGATGTCACTGTAATG	132
CCL20-R	GAATCCAGGAACAATGGTCAGT	
CRABP2-F	CTTTCTAAACGAGGGCAGGAT	171
CRABP2-R	TTTAAGGGAGCTGTTCAGGGT	
PLA2-F	AGACTCAAACGAGAGACGGGT	118
PLA2-R	TAGCAGGGTCGCAATGAGAG	
TNFRSF13C-F	TATTGCTGGTCTGTCGAGTGAGG	86
TNFRSF13C-R	CTTCAGTCTCTTACAGGCTTGGC	

Table 2. *Cont.*

Primer Name	Sequence (5′ to 3′)	Product Length (bp)
IgM-F	GCAAAGCCAAACACCCAAAT	88
IgM-R	CGAGCCGCAGACATTTTTCA	
EFNA5-F	CATTAGAACCAGCAGATGATACCG	82
EFNA5-R	CAAGACCCTGATGTTTTCTGTGAC	
CTSK-F	GAAGGAGAACAGGGGCATTGAC	92
CTSK-R	CGGCTGTAGAACTGGAAAGAGG	
β-actin-F	GAGACCTGACAGACTACCT	156
β-actin-R	AGGATGATGAAGCAGCAGT	

2.9. Statistical Analysis

All quantitative data were obtained from at least three independent experiments. The statistical significance of differences was analyzed by Student's *t* test using SPSS version 25 (IBM, Armonk, NY, USA). A significance threshold was set at $p < 0.05$. Graph assembly was visualized by GraphPad Prism version 8 software (GraphPad, San Diego, CA, USA).

3. Results

3.1. Histopathology

Notably, sections generated from all infected tissues showed shared features: necrotic cells, visible vacuolization, and bacterial accumulation in the tissues (Figure 1). The infected liver exhibited structurally disorganized hepatic lobules, hepatocellular necrosis and vacuolation, cell nuclear pyknosis and disappearance, and blurred cell outlines (Figure 1b). The infected spleen was characterized by a dramatic decrease in lymphocytes, lymphoid follicle hyperemia, and severe lymphatic necrosis and depletion (Figure 1d). Lymphocytic infiltration was observed in glomeruli and tubules, the number of renal tubules decreased, and tubules showed necrosis and atrophy (Figure 1f). Compared to the control group, the infected intestinal villi displayed fewer goblet cells and disordered absorptive cells. Structural disorder occurred in the lamina propria of the villi, with injured central chylomicron and loose muscle fibers (Figure 1h).

3.2. Toxigenic Profiles of B. cereus

According to our agarose gel electrophoretogram, *B. cereus* strain XS0724 carried several typical virulence factor genes, such as *NheA*, *NheB*, *NheC*, *HblA*, *HblC*, *HblD*, and *entFM*, but lacked *cytK* and *ces*. It is worth noting that although *bceT* primers amplified a

significant signal, it clearly did not match (>500 bp) the length of the target product (428 bp) (Figure 2).

3.3. Illumina Sequencing and de Novo Transcriptome Assembly

Qualified RNA was used for the sequencing library construction (Supplement Table S1). A total of 297 million raw reads were generated from the six cDNA libraries. The percentage of Q20 for each library was greater than 97% and Q30 was greater than 93%, indicating that the sequencing data was of high quality. A total of 277 million clean reads were obtained by removing low-quality reads and adaptor-contaminated reads (Table 3). The clean reads were assembled into 581,291 transcripts with a mean length of 904.31 bp and an N50 of 1877 bp. These transcripts were mapped to 348,665 unigenes with a mean length of 617.15 bp and an N50 of 892 bp (Table 4).
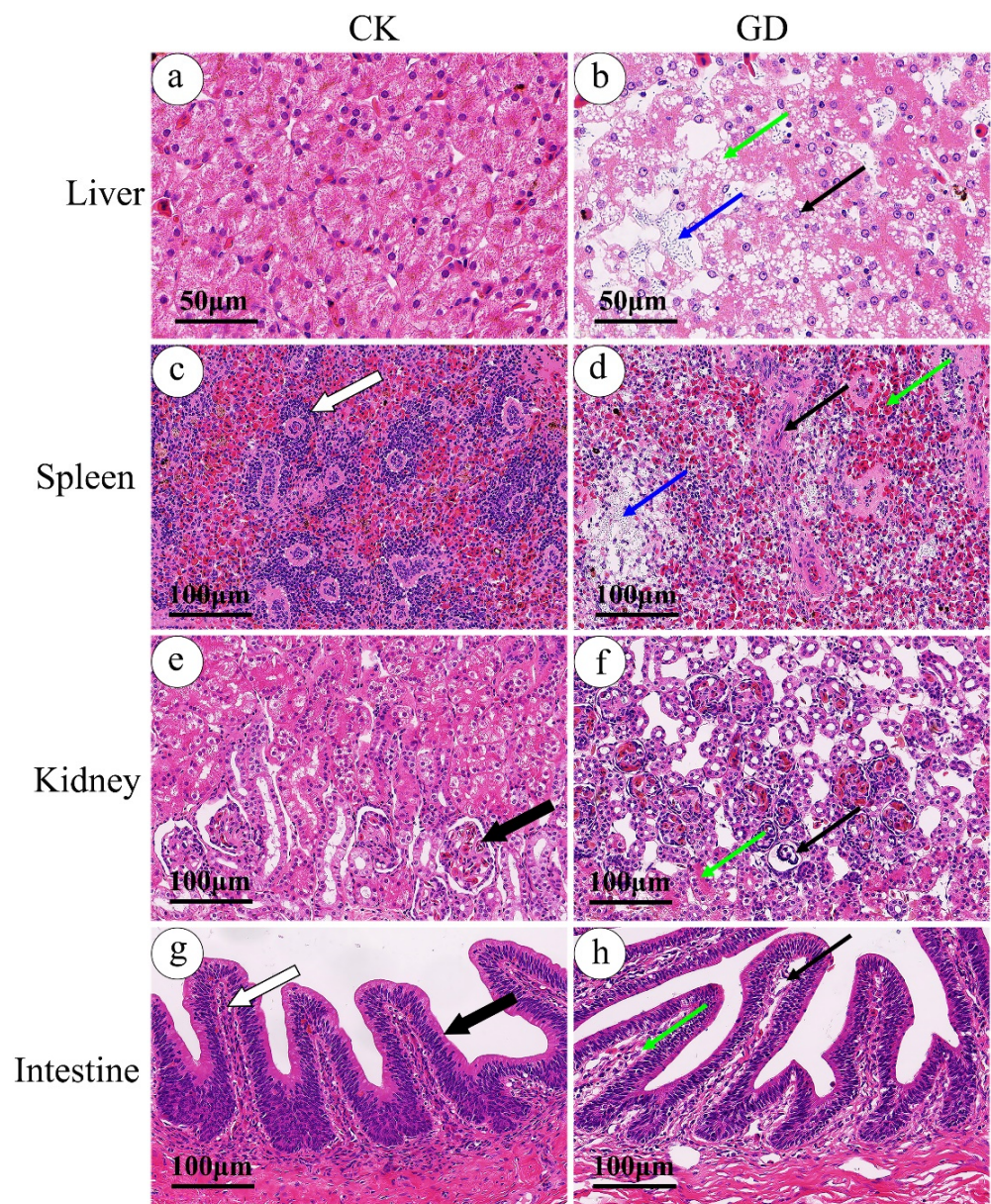
Figure 1. HE-stained histological sections of livers, spleens, kidneys, and intestines. CK and GD represent the control group and infection group, respectively. Scale bars denote a length of 50 (**a**,**b**) or 100 μm (**c**–**h**). The blue arrows point to bacterial accumulation universally. (**a**) The normal liver. (**b**) Collapse in a hepatic lobule (green arrow) and vacuolated cytoplasm due to nuclear pyknosis and karyolysis (black arrow). (**c**) Lymphoid follicle filled with an enormous number of lymphocytes in the control spleen (thick white arrow). (**d**) Atrophy and necrosis in a lymphoid follicle (black arrow) and overt hyperemia around lymphatic nodules (green arrow). (**e**) Healthy glomerulus with a distinct profile (thick black arrow). (**f**) Tubular necrosis (green arrow), and lymphocytic infiltrates and atrophy in glomeruli (black arrow). (**g**) The normal intestinal villi with morphologically normal lamina propria (thick white arrow) and goblet cells (thick black arrow). (**h**) Structural disorder of the lamina propria of the villi, with loose smooth muscle (green arrow) and damaged central chylomicron (black arrow).
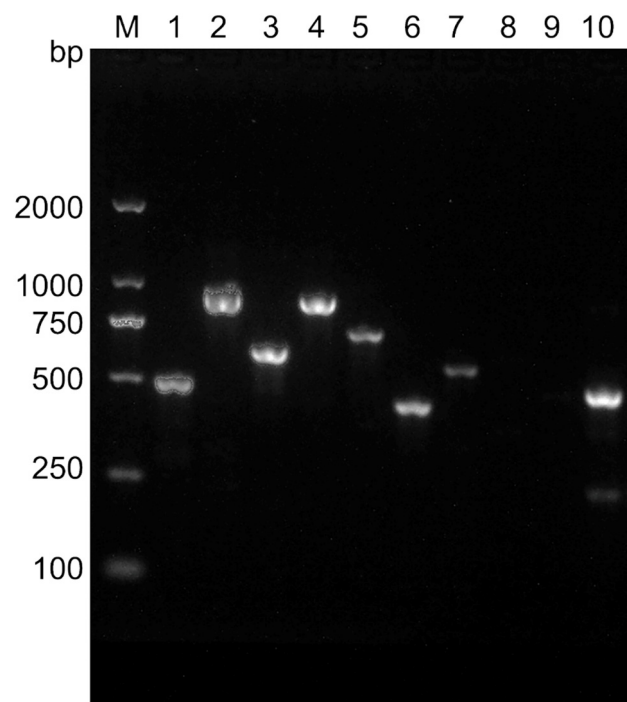
Figure 2. Gel electrophoretogram of virulence factor genes. Lane M represents the DL2000 DNA ladder marker. Lanes 1–10 represent *NheA*, *NheB*, *NheC*, *HblA*, *HblC*, *HblD*, *bceT*, *cytK*, *ces*, and *entFM*, respectively.

Table 3. Raw data statistics and filtering.

Sample	Raw Read Count	N (%)	Q20 (%)	Q30 (%)	Clean Read Count
GD1	52,733,514	0.001126	97.19	93.19	48,898,534
GD2	55,934,470	0.001126	97.17	93.27	51,912,132
GD3	43,562,612	0.001140	97.35	93.51	40,488,066
CK1	49,459,480	0.001144	97.37	93.50	46,319,408
CK2	47,077,210	0.001141	97.43	93.62	44,012,852
CK3	49,009,128	0.001136	97.28	93.37	45,907,658

Raw read count represents the total number of raw reads; N (%) represents the percentage of ambiguous bases; Q20 (%) represents the percentage of raw reads with a base recognition accuracy rate above 99%; Q30 (%) represents the percentage of raw reads with a base recognition accuracy rate above 99.9%; Clean read count represents the total number of clean reads.

Table 4. Summary of transcript assembly.

Category	Contigs	Transcripts	Unigenes
Total Length (bp)	301,124,798	525,666,538	215,178,805
Sequence Number	994,637	581,291	348,665
Max. Length (bp)	48,048	48,192	48,192
Mean Length (bp)	302.75	904.31	617.15
N50 (bp)	404	1877	892
N50 Sequence Number	140,096	73,705	50,754
N90 (bp)	140	311	255
N90 Sequence Number	737,917	368,926	253,811
GC (%)	47.00	48.19	47.16

N50 (bp): If all sequences are arranged from long to short and accumulated, when the accumulated length exceeds 50% of the total length of all sequences, the corresponding length of the last sequence is the N50; N90 has a similar definition to N50; GC (%) represents the GC content of the sequence.

3.4. Unigene Annotation

Among all unigenes, a total of 70,704 unigene sequences were annotated in six different databases. As shown in Table 5, 61,527 (17.65%), 25,656 (7.36%), 33,764 (9.68%) 15,315 (4.39%), 59,855 (17.17%), and 30,692 (8.80%) were annotated in the NR database, GO database, KEGG database, Pfam database, eggNOG database, and Swissprot database, respectively, and 7496 (2.15%) unigenes were matched to all databases. The homologous species (top hits upon a database search) distribution based on NR annotation revealed that 43.69% of the unigenes were highly similar to *T. sinensis*, which was more similar than *Chelonia mydas* (20.09%), *Chrysemys picta bellii* (10.99%), and others (Figure 3).

Table 5. Annotation statistics of unigenes in different databases.

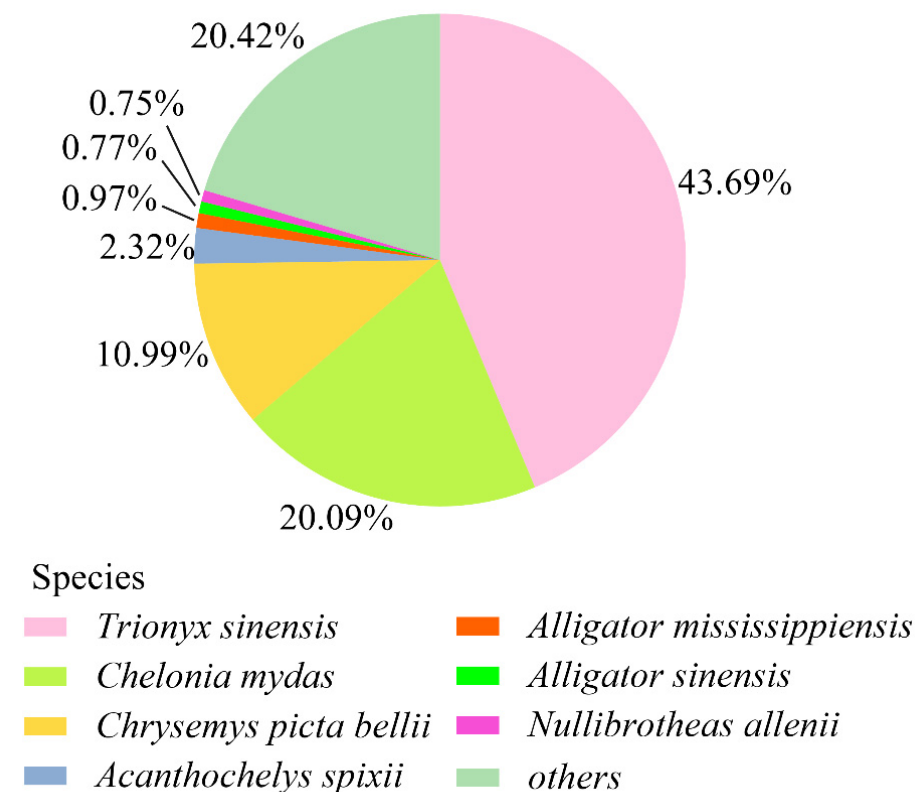| Database	Number	Percentage (%)
NR	61,527	17.65
GO	25,656	7.36
KEGG	33,764	9.68
Pfam	15,315	4.39
eggNOG	59,855	17.17
Swissprot	30,692	8.80
All databases	7496	2.15

Figure 3. The distribution of species for the best matched unigenes in the NR database. The pie chart shows the top seven species that were highly homologous to the unigene sequences matched in the NR database.

GO analysis can comprehensively clarify the biological function of unigenes. In the GO term annotation, a total of 25,656 unigenes were classified into three main categories: biological process, cellular component, and molecular function. Among the biological process subcategories, cellular process (GO:0009987), single-organism process (GO:0044699), and metabolic process (GO:0008152) were dominant. The predominant subcategories in cellular component were cell (GO:0005623), cell part (GO:0044464), and

membrane (GO:0016020). The most abundantly represented subcategories in molecular function were binding (GO:0005488), catalytic activity (GO:0003824), and transporter activity (GO:0005215) (Figure 4a).
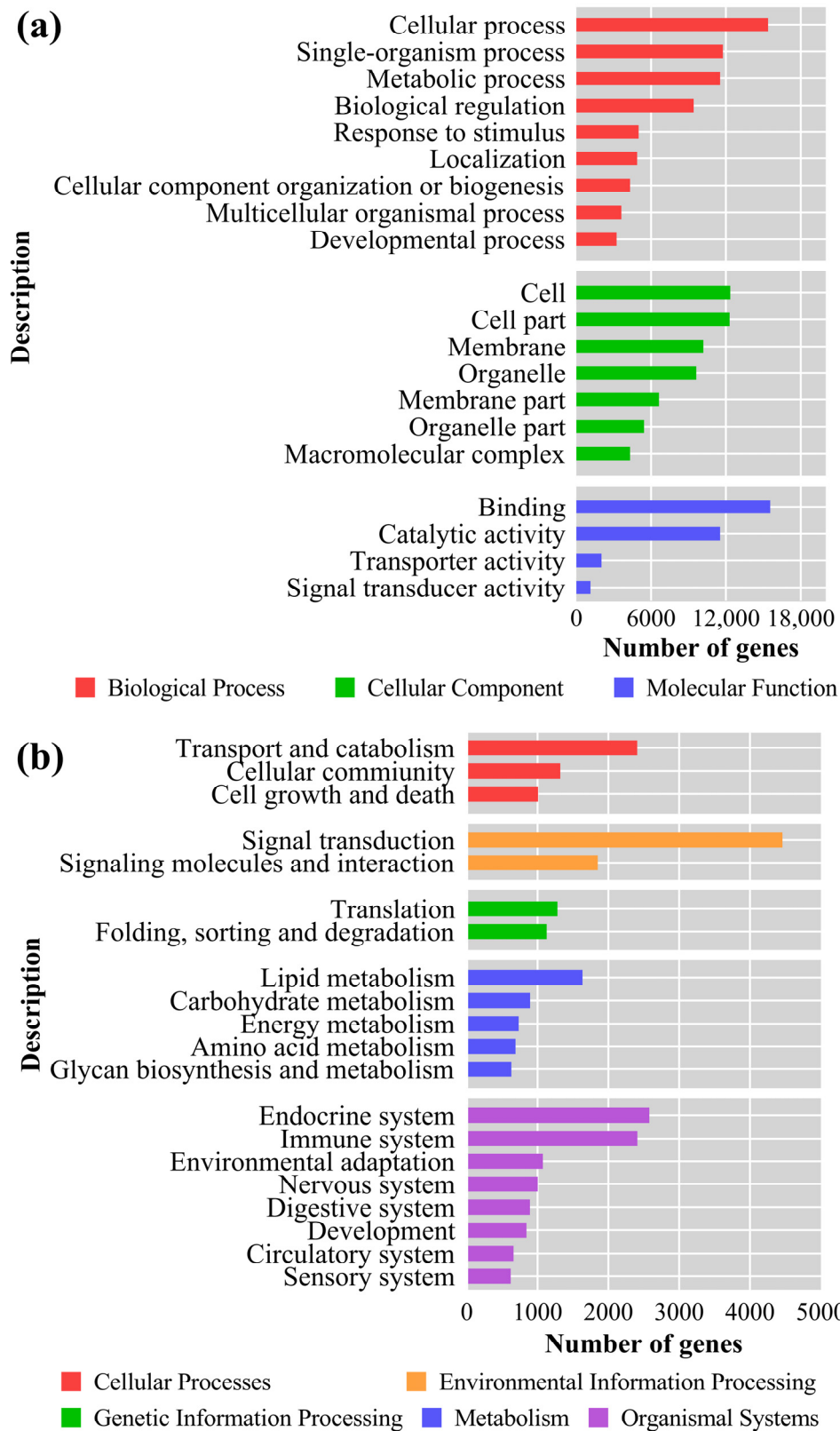

Figure 4. GO and KEGG category assignments of assembled unigenes. All unigenes were annotated into (**a**) three GO functional categories and (**b**) five KEGG categories.

To identify the KEGG pathways in *T. sinensis*, 33,764 annotated unigenes were assigned to multiple terms, primarily involving five broad categories: cellular processes, environmental information processing, genetic information processing, metabolism, and organismal systems. Furthermore, signal transduction, endocrine system, immune system, and transport and catabolism accounted for the main subcategories, containing 4457, 2579, 2409, and 2407 unigenes, respectively (Figure 4b).

The eggNOG annotation has an essential role in the functional description and functional classification of orthologous groups. Overall, a total of 59,855 unigenes were assigned to 26 eggNOG functional categories. Among them, the general function prediction only category (R; 26,773 unigenes) accounted for the major proportion, followed by the function unknown category (S; 13,267 unigenes), and the signal transduction mechanisms category (T; 7129 unigenes) (Table 6).

Table 6. The annotated eggNOG functions of unigenes.

Description	Category	Number of Unigenes
RNA processing and modification	A	891
Chromatin structure and dynamics	B	592
Energy production and conversion	C	912
Cell cycle control, cell division, chromosome partitioning	D	745
Amino acid transport and metabolism	E	660
Nucleotide transport and metabolism	F	438
Carbohydrate transport and metabolism	G	859
Coenzyme transport and metabolism	H	198
Lipid transport and metabolism	I	888
Translation, ribosomal structure, and biogenesis	J	1182
Transcription	K	3420
Replication, recombination, and repair	L	3983
Cell wall/membrane/envelope biogenesis	M	140
Cell motility	N	31
Posttranslational modification, protein turnover, chaperones	O	3251
Inorganic ion transport and metabolism	P	1015
Secondary metabolite biosynthesis, transport, and catabolism	Q	443
General function prediction only	R	26,773
Function unknown	S	13,267
Signal transduction mechanisms	T	7129
Intracellular trafficking, secretion, and vesicular transport	U	1561
Defense mechanisms	V	694
Extracellular structures	W	695
Undetermined	X	0
Nuclear structure	Y	88
Cytoskeleton	Z	1532

3.5. Analysis of the DEGs

To explore the mechanisms of the host response to *B. cereus* infection, DEGs were identified. All DEGs were displayed in a volcano plot (Figure 5a) and an MA plot (Figure 5b). Compared with the control group, a total of 18,593 genes were differentially expressed in the infected group, with 9678 upregulated genes and 8915 downregulated genes. A number of immune-related gene families were annotated and expressed differentially, mainly including immunoglobulins, antimicrobial peptides, nuclear factors, interferons, interleukins, complements, tumor necrosis factors, and chemokines (Table 7).
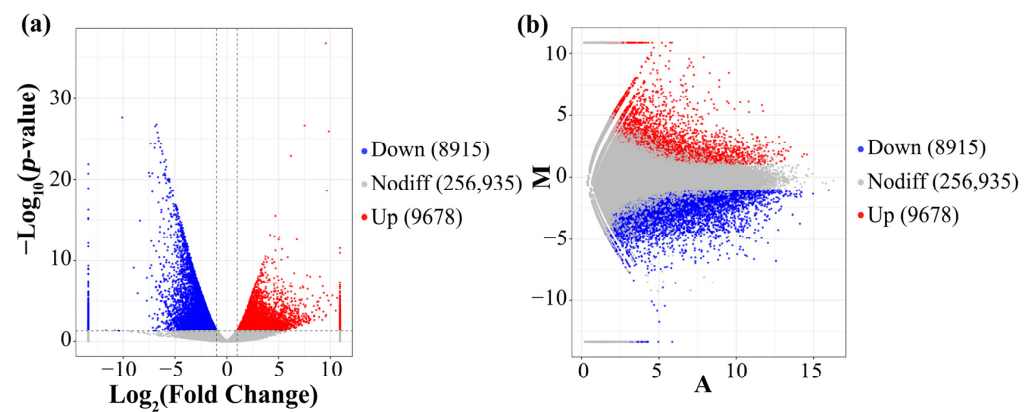
Figure 5. Statistical overview of DEGs. Each red dot represents a significantly upregulated gene, each blue dot represents a significantly downregulated gene, and each gray dot represents a non-significant differential gene. (**a**) Volcano plot of DEGs. The two vertical dashed lines indicate a fold change threshold of more than 2.0, while the horizontal dashed line indicates a *p*-value threshold lower than 0.05. (**b**) MA plot of DEGs. The X-axis represents the logarithm base 2 of the product of the gene expression in the two groups, while the Y-axis represents the logarithm of the fold change (base = 2).

Table 7. Information of immune-related DEGs in response to *B. cereus*.

Description	Fold Change	*p*-Value	Genebank
Immunoglobulin M heavy chain constant region	−2.22	4.35×10^{-2}	ACU45376.1
Immunoglobulin D heavy chain constant region	−20.27	1.30×10^{-5}	ACU45375.1
Immunoglobulin Y heavy chain constant region	−169.27	7.78×10^{-10}	ACU45374.1
Immunoglobulin superfamily member 8	−18.55	1.09×10^{-8}	XP_006115285.1
Immunoglobulin superfamily member 3-like	−2.72	3.08×10^{-2}	XP_014424150.1
Cathepsin D	−4.23	6.27×10^{-5}	XP_006134990.1
Cathepsin Z	−5.79	1.03×10^{-6}	XP_006134717.1
Cathepsin W-like	−8.21	4.41×10^{-3}	XP_006121731.2
Cathepsin S	−3.65	8.45×10^{-3}	XP_006110499.1
Cathepsin K-like	−11.17	2.53×10^{-2}	XP_006110501.1
Nuclear factor NF-kappa-B p105 subunit	+12.32	1.17×10^{-2}	XP_014430902.1
Nuclear factor of activated T-cells, cytoplasmic 1	−4.58	1.59×10^{-5}	XP_006128931.1
Nuclear factor NF-kappa-B p100 subunit	+12.00	7.84×10^{-3}	XP_006116288.1
Nuclear factor interleukin-3-regulated protein	+2.36	1.59×10^{-2}	XP_006131942.1
Interferon kappa-like	+7.54	1.07×10^{-2}	XP_006123052.1
Interferon-induced protein with tetratricopeptide repeats 5	+8.36	8.70×10^{-9}	XP_006121507.1
Interferon alpha-inducible protein 27-like protein 2B	+4.86	7.30×10^{-6}	XP_006113091.1
Interferon gamma receptor 1	−4.24	3.09×10^{-5}	XP_006112786.2
Stimulator of interferon genes protein	−4.33	2.35×10^{-5}	XP_014433634.1
Interferon-induced transmembrane protein 1-like	−2.37	1.37×10^{-2}	XP_006131716.1
Interferon-induced helicase C domain-containing protein 1	+2.40	1.55×10^{-2}	XP_006114909.1
Interferon regulatory factor 7	+5.46	1.76×10^{-2}	AHB33440.1
Interferon-induced protein with tetratricopeptide repeats 5-like	+2.19	1.84×10^{-2}	XP_014426629.1
Interferon gamma receptor 2	−2.07	3.06×10^{-2}	XP_006126153.1
Interleukin-12 subunit beta	+147.93	6.44×10^{-6}	XP_006138150.1
Interleukin-8-like	+71.18	1.33×10^{-4}	XP_006125459.1
Interleukin-6	+12.92	2.61×10^{-3}	XP_006138413.1
Interleukin-7	−3.68	3.32×10^{-4}	XP_014433210.1
Interleukin-20 receptor subunit alpha	−2.88	1.61×10^{-3}	XP_006112787.1
Interleukin-10-like	+2.43	1.31×10^{-2}	XP_006137332.1
Interleukin-5 receptor subunit alpha-like	−2.74	1.33×10^{-2}	XP_006135915.1
Interleukin-1 receptor-like 1	−21.26	6.43×10^{-7}	XP_006127707.1
Interleukin-22 receptor subunit alpha-2	−22.78	1.87×10^{-3}	XP_006112795.1
Toll-like receptor 9	−8.15	1.25×10^{-7}	XP_014427285.1

Table 7. *Cont.*

Description	Fold Change	*p*-Value	Genebank
Toll-like receptor 8	−6.19	1.19×10^{-6}	XP_006122907.1
Toll-like receptor 10	−5.22	4.70×10^{-3}	XP_014432216.1
Toll-like receptor 5	+3.08	7.33×10^{-3}	XP_006115662.2
Complement C1r subcomponent	+6.85	6.70×10^{-3}	XP_006130432.1
Complement receptor type 1-like	+3.31	9.58×10^{-4}	XP_006137323.1
Complement component C7 isoform X2	−36.21	2.45×10^{-19}	XP_006139554.1
Complement C1q subcomponent subunit A-like	−36.70	1.08×10^{-18}	XP_006121776.1
Tumor necrosis factor receptor superfamily member 1B	−4.51	1.30×10^{-5}	XP_014431383.1
Tumor necrosis factor receptor superfamily member 8	−7.21	1.63×10^{-4}	XP_006127981.1
Tumor necrosis factor receptor superfamily member 13B	−4.35	1.44×10^{-3}	XP_006126690.1
Tumor necrosis factor receptor superfamily member 13C	−11.18	3.67×10^{-3}	XP_006120590.1
Tumor necrosis factor ligand superfamily member 15	+2.47	5.97×10^{-3}	XP_006137247.1
Tumor necrosis factor receptor superfamily member 17	−5.00	1.23×10^{-2}	XP_014433201.1
C-C motif chemokine 20-like	+68.84	3.25×10^{-4}	XP_006119948.1
C-C motif chemokine 4-like	+54.47	2.01×10^{-4}	XP_006115931.1
C-C chemokine receptor type 9-like	−4.24	4.52×10^{-3}	XP_014434094.1
C-C chemokine receptor type 7	−4.57	1.11×10^{-4}	XP_014424601.1
Chemokine-like receptor 1	−6.10	2.98×10^{-5}	XP_006113767.1
C-C motif chemokine 3-like	−7.85	4.82×10^{-2}	XP_006115927.1
C-X-C chemokine receptor type 5	−16.60	1.11×10^{-4}	XP_006121016.1
C-X-C motif chemokine 14	−28.46	2.85×10^{-17}	XP_006116095.1

For fold change, "+" represents upregulation, "−" represents downregulation.

3.6. GO Analysis and KEGG Enrichment

GO enrichment analysis was further carried out to investigate the biological role of DEGs during *B. cereus* infection. A total of 3946 DEGs were enriched in 2174 GO terms: 1694 (77.92%) in the biological process category, 138 (6.35%) in the cellular component category, and 342 (15.73%) in the molecular function category. Response to stimulus (GO:0050896), cellular response to stimulus (GO:0051716), and multicellular organismal process (GO:0032501) were the three most enriched biological process GO terms. In the cellular component category, the top three terms were membrane part (GO:0044425), intrinsic component of membrane (GO:0031224), and integral component of membrane (GO:0016021). The three most represented terms enriched in the molecular function domain were receptor activity (GO:0004872), molecular transducer activity (GO:0060089), and signaling receptor activity (GO:0038023) (Figure 6).
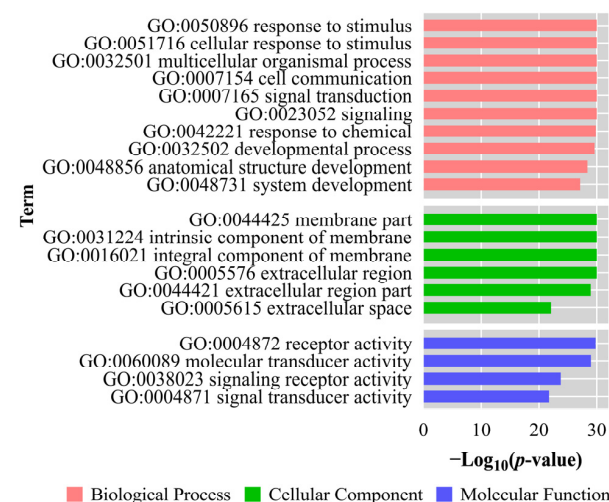

Figure 6. GO classification of DEGs after *B. cereus* infection. The top 20 terms of the three GO taxonomies, biological processes, cellular components, and molecular function, are presented.

For a systematic understanding of how *T. sinensis* responded to *B. cereus*, KEGG pathway enrichment analysis was further conducted. Overall, a total of 151 KEGG pathways were significantly enriched (p-value < 0.05), which were mainly involved in four categories: cellular processes, environmental information processing, human diseases, and organismal systems. Phagosome, NF-kappa B signaling pathway, rheumatoid arthritis, and hematopoietic cell lineage exhibited the most prominent enrichment in cellular processes, environmental information processing, human diseases, and organismal systems, respectively (Figure 7a). The top twenty KEGG pathways based on the lowest false discovery rates (FDRs) are shown in a bubble plot (Figure 7b).
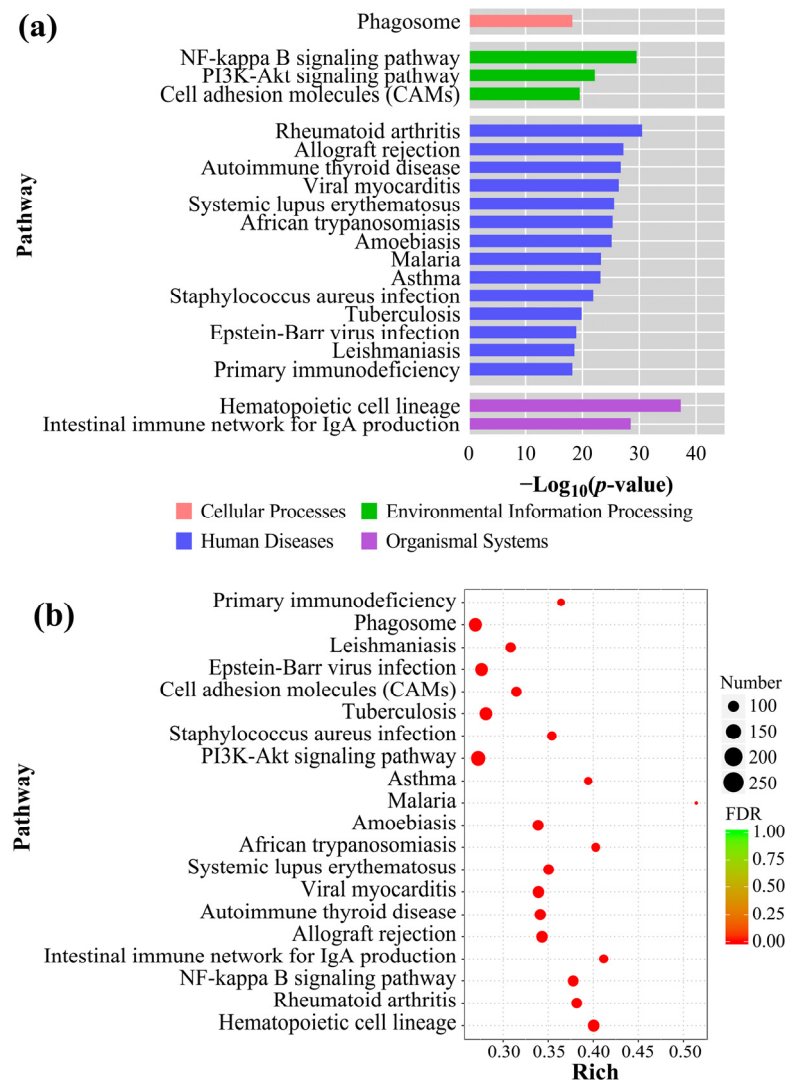
Figure 7. Classification and enrichment of DEGs mapped to KEGG pathways. (**a**) The top 20 KEGG pathways with the lowest p-value assigned in four categories. (**b**) Bubble plot of the top 20 enriched pathways based on the FDR values and the number of DEGs. The bubble size reflects the number of DEGs; the color of the bubble reflects the FDR, with a lower FDR indicating more significant enrichment.

3.7. Validation of RNA-Seq Data by qPCR

To further confirm the confidence and accuracy of transcriptome results, 11 immune-related genes were selected for qPCR validation, including six upregulated genes and five downregulated genes. Notably, a high consistency was observed between the transcriptome data and the qPCR results based on the correlation coefficient of 0.9617 and p-value < 0.001 (Figure 8).
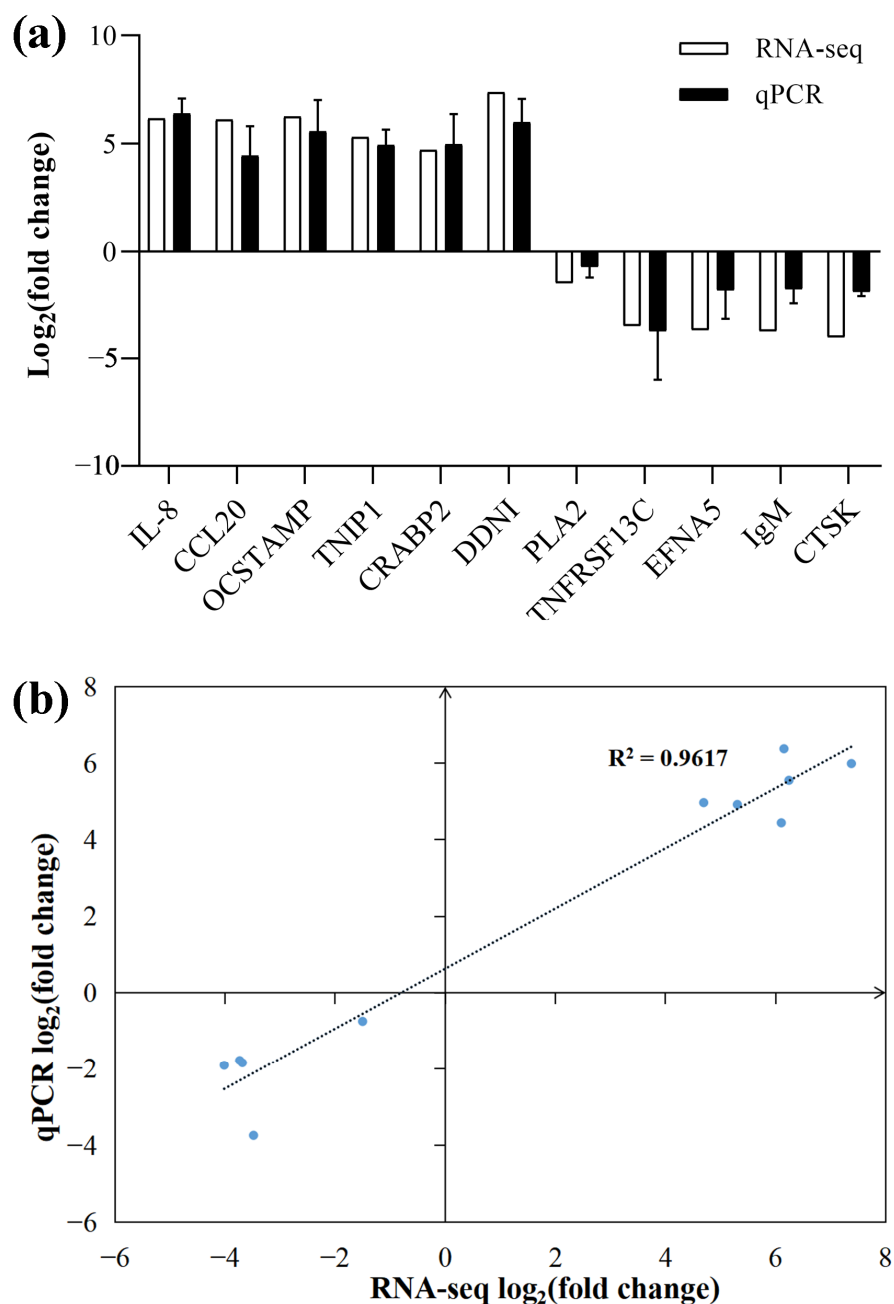
Figure 8. (**a**) Comparative analysis of RNA-seq data and qPCR at the transcript level. The standard deviations of the mean values from three qPCR replicates are visualized using error bars. (**b**) The linear regression of $\log_2$(fold-change) between qPCR data and RNA-seq data.

4. Discussion

4.1. Pathogenicity of B. cereus

B. cereus is generally regarded as a probiotic, and commonly used as an aquatic feed additive to promote growth and disease resistance [10,34]. However, growing evidence indicates that highly virulent strains could infect multiple aquatic animals, and cause gastrointestinal diseases in humans [35]. Histopathology is an intuitive approach to assessing pathogenic hazards and determining the organ damage mechanisms at the tissue level. Our results revealed an enormous number of necrotic cells and varying degrees of bleeding and bacterial accumulation in the liver, spleen, kidney, and intestine. A previous study found that *T. sinensis* infected with *B. cereus* suffered high mortality, accompanied by liver hemorrhage, splenomegaly, and intestinal edema [8]. A safety evaluation of commercial

B. cereus probiotics also found that some strains caused sepsis, liver injury, and intestinal inflammation in mice [36]. All these findings confirmed that virulent *B. cereus* could lead to serious organ damage in hosts, including *T. sinensis*.

We identified three types of virulence factor genes, *Nhes*, *Hbls*, and *entFM* in *B. cereus* strain XS0724. These virulence factor genes were also detected in *B. cereus* previously isolated from *T. sinensis* with high-mortality in Taiwan, China [8] and parrots in São Paulo, Brazil [37]. Nhe is one of the main members of the enterotoxins, and consists of NheA, NheB, and NheC. The enterotoxins can form an Nhe complex, which mediates holes in cell membranes and triggers cell lysis [38]. In our study, we speculated that cellular necrosis and vacuolization may be closely related to Nhe. As a hemolysin, Hbl is capable of hemolysis and altering vascular permeability [39]. This may be an important factor leading to visceral congestion and swelling found in our study. We also noted congestion in the lungs, liver, heart, kidneys, intestines, and spleens [37]. Highly similar symptoms suggested that the bacteria were indeed attacking the diseased organs. EntFM is involved in bacterial movement and shape, adhesion, biofilm formation, and vacuolization of macrophages [40]. The *bceT*, *cytK*, and *ces* genes have been detected in *B. cereus* from other sources [8,37,41–43]. However, *B. cereus* strain XS0724 presented an absence of the commonly found *bceT*, *cytK*, and *ces* genes in our study. This revealed differences in virulence factors among *B. cereus* from different sources, possibly due to specificity in host-pathogen affinity and variability from environmental adaptations [44].

4.2. Immune-Related DEGs

To further understand the response mechanism of immune organs to *B. cereus* infection, we systematically dissected the transcriptome of the spleen. A total of 18,593 differentially expressed genes were identified, including 9678 upregulated genes and 8915 downregulated genes, which was more than in the lung tissue of *T. sinensis* infected by *Trionyx sinensis* hemorrhagic syndrome virus [32]. DEGs showed high diversity, especially in immune-related genes. The diverse genes initially indicated that bacterial infections triggered complex immune activities.

Interleukin-6 (IL-6), a pleiotropic pro-inflammatory cytokine, plays a pivotal role in inducing the proliferation and expansion of lymphocytes [45]. In our experiments, *IL-6* mRNA level was significantly upregulated in response to infection. Upon pathogen recognition, the similar up-regulation of *IL-6* mRNA level was observed in the spleen leukocytes, indicating that *IL-6* mRNA might be involved in host defense against bacterial infection [46]. IL-6 is used as a typical inflammatory biomarker to predict diseases in humans, considering its rapid induction during inflammation and cancer [47,48].

IL-8, also referred to as CXCL8, is responsible for neutrophil recruitment, activation, and chemotaxis [49]. In our results, *IL-8* mRNA expression was significantly upregulated in response to *B. cereus* infection. A previous study found that *IL-8* mRNA was constitutively expressed in different tissues, and was upregulated particularly in the spleen after bacterial infection [50]. All these findings suggested that the spleen and *IL-8* might contribute to the antimicrobial response. Similar to avian species, *T. sinensis* can express *IL-8* mRNA containing an ELR motif [50], which has been found to promote angiogenesis [51]. We speculated that upregulation of *IL-8* mRNA expression may compensate for visceral hemorrhage after infection.

Chemokines are confirmed to stimulate leukocyte migration and activation during an immuno-inflammatory response [52]. CCL20 plays an important role in the migration of Th17 cells and regulatory T cells to inflammatory sites and can also induce IL-17 production [53]. The prominent upregulation of *CCL20* mRNA expression with bacterial infection in this study may suggest the activation of the inflammatory response after bacterial infection. CCL20 chemokine displayed antibacterial activities in *Micropterus salmoides* challenge with *Nocardia seriolae* [54], which may be relative to its electrostatic surface topology [55]. This may explain the changes of *CCL20* mRNA level in our study. CCL20 can only bind to the specific receptor CCR6 to form the CCL20-CCR6 axis [56]. Moreover, B cells with a

higher CCR6 expression level showed a higher CCL20 expression level [57]. In this study, we did not find a high expression level of *CCR6* mRNA but did for *CCL20* mRNA. It was possible that the CCL20-CCR6 axis was not activated. Further research is needed to clarify the detailed mechanism.

The complement system is a critical part of immune reactions and contributes to defense against invading pathogens [58]. Complement activation enhances pathogen lysis, phagocytosis, clearance of apoptotic bodies, and cytokine production [59]. Our results showed that the *C1r* mRNA level was increased after infection, but *C7* and *C1q* mRNA levels were downregulated, in contradiction with previous reports [60,61]. The binding of C1q to immunoglobulin triggers the subsequent efficient activation of C1, the first component of the complement system [62]. The activation of C7 can lead to the membrane attack complex (MAC) on the target membrane, which ultimately contributes to the disruption of bacterial cell walls, cell lysis, and osmotic imbalance [63]. It could be predicted that C7 might have antibacterial effects in *T. sinensis*. Our results, however, suggested that *T. sinensis* had a weak complement response to *B. cereus* infection. This may be explained by differences in host and pathogen stimuli. Noting previous studies, although the complement system was not significantly activated in this research, it was possible that complement components indirectly stimulated immune responses through inflammation, adaptive immunity, and tissue repair [64,65].

4.3. Immune-Related Pathways

Pathway analysis helps to elucidate molecular immune mechanisms and associations more clearly and purposefully because pathways are the relationship network among genes. In the KEGG enrichment analysis, the primary pathways related to the immune response were phagosome, NF-kappa B signaling pathway, PI3K-Akt signaling pathway, cell adhesion molecules (CAMs), and hematopoietic cell lineage. These enriched pathways may be involved in the antimicrobial and inflammatory responses in the spleen of *T. sinensis* infected by *B. cereus.* Similar pathways were also reported in previous studies [66–68].

The phagosome signaling pathway is considered as one of the most common mechanisms of eliminating exogenous microorganisms [69]. Phagosomes mainly occur in several specialized phagocytic cells, such as macrophages, monocytes, neutrophils, and dendritic cells (DCs) [70]. In macrophages, mature phagosomes can kill internalized microorganisms, and degrade and remove cell debris [71]. In DCs, phagocytes effectively prevent degradation of the antigenic peptides, allowing the major histocompatibility complex (MHC) to participate in antigen presentation [72]. In rainbow trout, the phagosome pathway was activated and MHC1 was upregulated in the spleen to resist *Yersinia ruckeri* infection [73]. In addition, it has been reported that phagosomes have a superior ability to present antigens through MHC II by generating degraded exogenous peptides from microorganisms bound to TLR ligands [74]. Therefore, the significant enrichment of the phagosome pathways in this study indicated that the host effectively promoted microbial degradation and stimulated the immune response against microbial invasion.

It is noteworthy that in addition to the phagosome pathway, the NF-κB pathway also participated in the antibacterial response in *T. sinensis*. The NF-κB pathway is regarded as a canonical proinflammatory signaling pathway [75]. Nuclear factor-κB (NF-κB) is composed of several transcription factors. Under unstimulated conditions, NF-κB is an inactive dimer due to the inhibitor of NF-κB proteins (IκBs) [76]. NF-κB is activated by lipopolysaccharide and proinflammatory cytokines under exogenous *B. cereus* infection [77], and translocates to the nucleus to promote the transcription of targeted genes [78]. The target genes cover a variety of cytokines, such as interleukins, chemokines, adhesion molecules, acute phase proteins, and inflammatory enzymes [79]. Differentially expressed inflammatory cytokines were found in our results, some of which may be mediated by the pro-inflammatory effects of the NF-κB pathway. The enrichment of the NF-κB pathway suggested that it played a crucial part in the inflammatory response against *B. cereus* infection. It has been reported that the promoter region of the serum amyloid A (a major acute phase protein) gene in

T. sinensis contains an NF-κB binding site [80], suggesting that NF-κB is also critical in regulating the acute phase reaction.

5. Conclusions

In this study, we evaluated the pathogenicity of *B. cereus*. Histopathological observations and the detection of virulence factor genes confirmed severe damage at the tissue level and revealed pathogenic molecules. Furthermore, for the first time, we presented the transcriptome profile of the spleen in *T. sinensis* with *B. cereus* infection, and identified multiple immune-related genes involved in the phagosome, NF-kappa B signaling pathway, PI3K-Akt signaling pathway, and cell adhesion molecules (CAMs). These results contributed to enriching our understanding of the immune mechanisms of *T. sinensis* against *B. cereus*, providing opportunities for developing novel strategies in the prevention of this disease in the future.

References

1. Park, S.B.; Aoki, T.; Jung, T.S. Pathogenesis of and strategies for preventing *Edwardsiella tarda* infection in fish. *Vet. Res.* **2012**, *43*, 67. [CrossRef] [PubMed]
2. Zhao, W.; Dao, C.; Karim, M.; Gomez-Chiarri, M.; Rowley, D.; Nelson, D.R. Contributions of tropodithietic acid and biofilm formation to the probiotic activity of *Phaeobacter inhibens*. *BMC Microbiol.* **2016**, *16*, 1–17. [CrossRef] [PubMed]
3. Defoirdt, T.; Sorgeloos, P.; Bossier, P. Alternatives to antibiotics for the control of bacterial disease in aquaculture. *Curr. Opin. Microbiol.* **2011**, *14*, 251–258. [CrossRef] [PubMed]
4. Munang'andu, H.M. Intracellular bacterial infections: A challenge for developing cellular mediated immunity vaccines for farmed fish. *Microorganisms* **2018**, *6*, 33. [CrossRef]
5. Chen, J.S.; Zhu, N.Y.; Kong, L.; Bei, Y.J.; Zheng, T.L.; Ding, X.Y.; He, Z.Y. First case of soft shell disease in Chinese soft-shelled turtle (*Trionyx sinens*) associated with *Aeromonas sobria-A. veronii* complex. *Aquaculture* **2013**, *406*, 62–67. [CrossRef]
6. Chung, T.H.; Yi, S.W.; Kim, B.S.; Kim, W.I.; Shin, G.W. Identification and antibiotic resistance profiling of bacterial isolates from septicaemic soft-shelled turtles (*Pelodiscus sinensis*). *Vet. Med.* **2017**, *62*, 169–177. [CrossRef]
7. Liu, L.; Cao, Z.; Lin, F.; Ye, X.P.; Lu, S.J.; Lyv, S.J. The histopathological characteristics caused by *Trionyx sinensis* hemorrhagic syndrome virus (TSHSV) and comparative proteomic analysis of liver tissue in TSHSV-infected chinese soft-shelled turtles (*Pelodiscus sinensis*). *Intervirology* **2017**, *60*, 19–27. [CrossRef]
8. Cheng, L.W.; Rao, S.; Poudyal, S.; Wang, P.C.; Chen, S.C. Genotype and virulence gene analyses of *Bacillus cereus* group clinical isolates from the Chinese softshell turtle (*Pelodiscus sinensis*) in Taiwan. *J. Fish Dis.* **2021**, *44*, 1515–1529. [CrossRef]
9. Stenfors Arnesen, L.P.; Fagerlund, A.; Granum, P.E. From soil to gut: *Bacillus cereus* and its food poisoning toxins. *FEMS Microbiol. Rev.* **2008**, *32*, 579–606. [CrossRef]
10. Li, H.D.; Fan, S.L.; Gao, Y.; Cai, Y.Y.; Chu, Z.J.; Wang, L. Evaluation of modulatory properties of *Bacillus cereus* isolated from the gut of *Litopenaeus vannamai* on growth, intestinal morphology, digestive enzyme activities, immune responses and disease resistance of *Litopenaeus vannamai*. *Aquacult. Res.* **2021**, *52*, 1299–1310. [CrossRef]

11. Jovanovic, J.; Ornelis, V.F.M.; Madder, A.; Rajkovic, A. *Bacillus cereus* food intoxication and toxicoinfection. *Compr. Rev. Food Sci. Food Saf.* **2021**, *20*, 3719–3761. [CrossRef] [PubMed]

12. Velmurugan, S.; Palanikumar, P.; Velayuthani, P.; Donio, M.B.S.; Babu, M.M.; Lelin, C.; Sudhakar, S.; Citarasu, T. Bacterial white patch disease caused by *Bacillus cereus*, a new emerging disease in semi-intensive culture of *Litopenaeus vannamei*. *Aquaculture* **2015**, *444*, 49–54. [CrossRef]

13. Zhang, Z.; Zhang, W.; Hu, Z.; Li, C.; Shao, Y.; Zhao, X.; Guo, M. Environmental factors promote pathogen-induced skin ulceration syndrome outbreak by readjusting the hindgut microbiome of *Apostichopus japonicus*. *Aquaculture* **2019**, *507*, 155–163. [CrossRef]

14. Li, Y.L.; Zhang, H.Q.; Lv, S.J.; Lin, F.; Liu, L.; Yuan, X.M.; Su, S.Q. Isolation and identification of pathogen causing "head-shaking syndrome" of *Pelodiscus sinensis nigrum* and drug susceptibility analysis. *Oceanol. Limnol. Sin.* **2020**, *51*, 405–414. [CrossRef]

15. Yuan, X.M.; Lyu, S.J.; Zhang, H.Q.; Hang, X.Y.; Shi, W.D.; Liu, L.; Wu, Y.L. Complete genome sequence of novel isolate SYJ15 of *Bacillus cereus* group, a highly lethal pathogen isolated from Chinese soft shell turtle (*Pelodiscus Sinensis*). *Arch. Microbiol.* **2020**, *202*, 85–92. [CrossRef]

16. Zhu, C.K.; Pan, Z.J.; Chang, G.L.; Wu, N.; Wang, H.; Ding, H.Y.; Qiang, X.G.; Zhang, L.; Qiang, J.; Zhang, J.; et al. Transcriptomic insights into immune responses to ulcerative syndrome in *Pseudobagrus ussuriensis*. *Aquaculture* **2021**, *537*, 736504. [CrossRef]

17. Qi, Z.T.; Zhang, Q.H.; Wang, Z.S.; Ma, T.Y.; Zhou, J.; Holland, J.W.; Gao, Q. Transcriptome analysis of the endangered Chinese giant salamander (*Andrias davidianus*): Immune modulation in response to *Aeromonas hydrophila* infection. *Vet. Immunol. Immunopathol.* **2016**, *169*, 85–95. [CrossRef]

18. Wang, D.; Sun, S.M.; Li, S.W.; Lu, T.Y.; Shi, D.F. Transcriptome profiling of immune response to *Yersinia ruckeri* in spleen of rainbow trout (*Oncorhynchus mykiss*). *BMC Genom.* **2021**, *22*, 292. [CrossRef]

19. Fischer, A.H.; Jacobson, K.A.; Rose, J.; Zeller, R. Hematoxylin and eosin staining of tissue and cell sections. *Cold Spring Harb. Protoc.* **2008**, *2008*, pdb.prot4986. [CrossRef]

20. Hansen, B.M.; Hendriksen, N.B. Detection of enterotoxic *Bacillus cereus* and *Bacillus thuringiensis* strains by PCR analysis. *Appl. Environ. Microbiol.* **2001**, *67*, 185–189. [CrossRef]

21. Ngamwongsatit, P.; Buasri, W.; Pianariyanon, P.; Pulsrikarn, C.; Ohba, M.; Assavanig, A.; Panbangred, W. Broad distribution of enterotoxin genes (*hblCDA*, *nheABC*, *cytK*, and *entFM*) among *Bacillus thuringiensis* and *Bacillus cereus* as shown by novel primers. *Int. J. Food Microbiol.* **2008**, *121*, 352–356. [CrossRef] [PubMed]

22. Agata, N.; Ohta, M.; Arakawa, Y.; Mori, M. The *bceT* gene of *Bacillus cereus* encodes an enterotoxic protein. *Microbiology* **1995**, *141*, 983–988. [CrossRef] [PubMed]

23. Kim, G.H.; Forghani, F.; Oh, D.H. Rapid detection of emetic toxin producing *Bacillus cereus* strains using triple-primer polymerase chain reaction (PCR) assay. *Afr. J. Microbiol. Res.* **2013**, *7*, 620–625. [CrossRef]

24. Grabherr, M.G.; Haas, B.J.; Yassour, M.; Levin, J.Z.; Thompson, D.A.; Amit, I.; Adiconis, X.; Fan, L.; Raychowdhury, R.; Zeng, Q.; et al. Full-length transcriptome assembly from RNA-Seq data without a reference genome. *Nat. Biotechnol.* **2011**, *29*, 644–652. [CrossRef] [PubMed]

25. Buchfink, B.; Xie, C.; Huson, D.H. Fast and sensitive protein alignment using DIAMOND. *Nat. Methods* **2015**, *12*, 59–60. [CrossRef] [PubMed]

26. Götz, S.; García-Gómez, J.M.; Terol, J.; Williams, T.D.; Nagaraj, S.H.; Nueda, M.J.; Robles, M.; Talón, M.; Dopazo, J.; Conesa, A. High-throughput functional annotation and data mining with the Blast2GO suite. *Nucleic Acids Res.* **2008**, *36*, 3420–3435. [CrossRef]

27. Moriya, Y.; Itoh, M.; Okuda, S.; Yoshizawa, A.C.; Kanehisa, M. KAAS: An automatic genome annotation and pathway reconstruction server. *Nucleic Acids Res.* **2007**, *35*, W182–W185. [CrossRef]

28. Li, B.; Dewey, C.N. RSEM: Accurate transcript quantification from RNA-Seq data with or without a reference genome. *BMC Bioinf.* **2011**, *12*, 323. [CrossRef]

29. Anders, S.; McCarthy, D.J.; Chen, Y.; Okoniewski, M.; Smyth, G.K.; Huber, W.; Robinson, M.D. Count-based differential expression analysis of RNA sequencing data using R and Bioconductor. *Nat. Protoc.* **2013**, *8*, 1765–1786. [CrossRef]

30. Benjamini, Y.; Hochberg, Y. Controlling the false discovery rate: A practical and powerful approach to multiple testing. *J. R. Stat. Soc. Ser. B Stat. Methodol.* **1995**, *57*, 289–300. [CrossRef]

31. Mao, X.; Cai, T.; Olyarchuk, J.G.; Wei, L. Automated genome annotation and pathway identification using the KEGG Orthology (KO) as a controlled vocabulary. *Bioinformatics* **2005**, *21*, 3787–3793. [CrossRef] [PubMed]

32. Lyu, S.J.; Yuan, X.M.; Zhang, H.Q.; Hang, X.Y.; Li, Y.L.; Shi, W.D.; Liu, L.; Yu, Z.; Wu, Y.L. Transcriptome profiling analysis of lung tissue of Chinese soft-shell turtle infected by *Trionyx sinensis* hemorrhagic syndrome virus. *Fish Shellfish Immunol.* **2020**, *98*, 653–660. [CrossRef] [PubMed]

33. Livak, K.J.; Schmittgen, T.D. Analysis of relative gene expression data using real-time quantitative PCR and the $2^{-\Delta\Delta CT}$ method. *Methods* **2001**, *25*, 402–408. [CrossRef] [PubMed]

34. Muthukrishnan, S.; Hoong, M.C.; Chen, W.W.; Natrah, I. Efficacy of *Bacillus cereus* strain BP-MBRG/1b and prebiotic fructooligosaccharides dietary supplementation on growth performance and disease resistance of *Macrobrachium rosenbergii* (De Mann) towards *Aeromonas hydrophila* AH-1N. *Aquacult. Res.* **2021**, *52*, 1657–1665. [CrossRef]

35. Al-Khatib, M.S.; Khyami-Horani, H.; Badran, E.; Shehabi, A.A. Incidence and characterization of diarrheal enterotoxins of fecal *Bacillus cereus* isolates associated with diarrhea. *Diagn. Microbiol. Infect. Dis.* **2007**, *59*, 383–387. [CrossRef] [PubMed]

36. Cui, Y.F.; Wang, S.L.; Ding, S.Y.; Shen, J.Z.; Kui, Z. Toxins and mobile antimicrobial resistance genes in *Bacillus* probiotics constitute a potential risk for one health. *J. Hazard. Mater.* **2020**, *382*, 121266. [CrossRef]

37. Godoy, S.N.; Matushima, E.R.; Chaves, J.Q.; Cavados, C.F.; Rabinovitch, L.; Teixeira, R.H.; Nunes, A.L.; Melville, P.; Gattamorta, M.A.; Vivoni, A.M. *Bacillus cereus* infection outbreak in captive psittacines. *Vet. Microbiol.* **2012**, *161*, 213–217. [CrossRef]

38. Fagerlund, A.; Lindbäck, T.; Storset, A.K.; Granum, P.E.; Hardy, S.P. *Bacillus cereus* Nhe is a pore-forming toxin with structural and functional properties similar to the ClyA (HlyE, SheA) family of haemolysins, able to induce osmotic lysis in epithelia. *Microbiology* **2008**, *154*, 693–704. [CrossRef]

39. Beecher, D.J.; Schoeni, J.L.; Wong, A.C. Enterotoxic activity of hemolysin BL from *Bacillus cereus*. *Infect. Immun.* **1995**, *63*, 4423–4428. [CrossRef]

40. Tran, S.L.; Guillemet, E.; Gohar, M.; Lereclus, D.; Ramarao, N. CwpFM (EntFM) is a *Bacillus cereus* potential cell wall peptidase implicated in adhesion, biofilm formation, and virulence. *J. Bacteriol.* **2010**, *192*, 2638–2642. [CrossRef]

41. Nfor, N.N.; Lapin, C.N.; McLaughlin, R.W. Isolation of *Bacillus cereus* group from the fecal material of endangered wood turtles. *Curr. Microbiol.* **2015**, *71*, 524–527. [CrossRef]

42. Hsu, T.K.; Tsai, H.C.; Hsu, B.M.; Yang, Y.Y.; Chen, J.S. Prevalence, enterotoxin-gene profiles, antimicrobial resistance, and genetic diversity of *Bacillus cereus* group in aquatic environments and shellfish. *Sci. Total Environ.* **2021**, *758*, 143665. [CrossRef] [PubMed]

43. Zhao, S.J.; Chen, J.L.; Fei, P.; Feng, H.X.; Wang, Y.; Ali, M.; Li, S.Z.; Jing, H.N.; Yang, W.W. Prevalence, molecular characterization, and antibiotic susceptibility of *Bacillus cereus* isolated from dairy products in China. *J. Dairy Sci.* **2020**, *103*, 3994–4001. [CrossRef] [PubMed]

44. Ceuppens, S.; Boon, N.; Uyttendaele, M. Diversity of *Bacillus cereus* group strains is reflected in their broad range of pathogenicity and diverse ecological lifestyles. *FEMS Microbiol. Ecol.* **2013**, *84*, 433–450. [CrossRef] [PubMed]

45. Li, B.; Jones, L.L.; Geiger, T.L. IL-6 promotes T cell proliferation and expansion under inflammatory conditions in association with low-level RORγt expression. *J. Immunol.* **2018**, *201*, 2934–2946. [CrossRef] [PubMed]

46. Wei, X.; Li, B.; Wu, L.; Yin, X.; Zhong, X.; Li, Y.; Wang, Y.; Guo, Z.; Ye, J. Interleukin-6 gets involved in response to bacterial infection and promotes antibody production in Nile tilapia (*Oreochromis niloticus*). *Dev. Comp. Immunol.* **2018**, *89*, 141–151. [CrossRef]

47. Unver, N.; McAllister, F. IL-6 family cytokines: Key inflammatory mediators as biomarkers and potential therapeutic targets. *Cytokine Growth Factor Rev.* **2018**, *41*, 10–17. [CrossRef]

48. Ma, Y.; Ren, Y.; Dai, Z.J.; Wu, C.J.; Ji, Y.H.; Xu, J. IL-6, IL-8 and TNF-α levels correlate with disease stage in breast cancer patients. *Adv. Clin. Exp. Med.* **2017**, *26*, 421–426. [CrossRef]

49. Das, S.T.; Rajagopalan, L.; Guerrero-Plata, A.; Sai, J.; Richmond, A.; Garofalo, R.P.; Rajarathnam, K. Monomeric and dimeric CXCL8 are both essential for in vivo neutrophil recruitment. *PLoS ONE* **2010**, *5*, e11754. [CrossRef]

50. Zhou, X.X.; Guo, Q.L.; Dai, H.P. Molecular characterization and expression profiles in response to bacterial infection of Chinese soft-shelled turtle interleukin-8 (IL-8), the first reptilian chemokine gene. *Dev. Comp. Immunol.* **2009**, *33*, 838–847. [CrossRef]

51. Strieter, R.M.; Polverini, P.J.; Kunkel, S.L.; Arenberg, D.A.; Burdick, M.D.; Kasper, J.; Dzuiba, J.; Van Damme, J.; Walz, A.; Marriott, D.; et al. The functional role of the ELR motif in CXC chemokine-mediated angiogenesis. *J. Biol. Chem.* **1995**, *270*, 27348–27357. [CrossRef] [PubMed]

52. Laufer, J.M.; Legler, D.F. Beyond migration-chemokines in lymphocyte priming, differentiation, and modulating effector functions. *J. Leukoc. Biol.* **2018**, *104*, 301–312. [CrossRef]

53. Yamazaki, T.; Yang, X.O.; Chung, Y.; Fukunaga, A.; Nurieva, R.; Pappu, B.; Martin-Orozco, N.; Kang, H.S.; Ma, L.; Panopoulos, A.D.; et al. CCR6 regulates the migration of inflammatory and regulatory T cells. *J. Immunol.* **2008**, *181*, 8391–8401. [CrossRef] [PubMed]

54. Byadgi, O.; Chen, C.W.; Wang, P.C.; Tsai, M.A.; Chen, S.C. De novo transcriptome analysis of differential functional gene expression in largemouth bass (*Micropterus salmoides*) after challenge with *Nocardia seriolae*. *Int. J. Mol. Sci.* **2016**, *17*, 1315. [CrossRef] [PubMed]

55. Liu, F.; Wang, T.; Hu, Y.; Tian, G.; Secombes, C.J.; Wang, T. Expansion of fish CCL20_like chemokines by genome and local gene duplication: Characterisation and expression analysis of 10 CCL20_like chemokines in rainbow trout (*Oncorhynchus mykiss*). *Dev. Comp. Immunol.* **2020**, *103*, 103502. [CrossRef] [PubMed]

56. Schutyser, E.; Struyf, S.; Van Damme, J. The CC chemokine CCL20 and its receptor CCR6. *Cytokine Growth Factor Rev.* **2003**, *14*, 409–426. [CrossRef]

57. Chang, K.C.; Chen, R.Y.; Wang, Y.C.; Hung, L.Y.; Medeiros, L.J.; Chen, Y.P.; Chen, T.Y.; Yang, J.C.; Chiang, P.M. Stem cell characteristics promote aggressiveness of diffuse large B-cell lymphoma. *Sci. Rep.* **2020**, *10*, 21342. [CrossRef]

58. Hawksworth, O.A.; Coulthard, L.G.; Woodruff, T.M. Complement in the fundamental processes of the cell. *Mol. Immunol.* **2017**, *84*, 17–25. [CrossRef]

59. Thurman, J.M.; Holers, V.M. The central role of the alternative complement pathway in human disease. *J. Immunol.* **2006**, *176*, 1305–1310. [CrossRef]

60. Li, F.; Liu, X.; Ge, H.; Huang, J.; Zhang, Y.; Wang, Z. Transcriptome profiling and differential expression analysis of the immune-related genes during the early phase of acute infection with *Aeromonas hydrophila* in the Chinese sucker (*Myxocyprinus asiaticus*). *Aquaculture* **2021**, *545*, 737258. [CrossRef]

61. Dang, Y.; Xu, X.; Shen, Y.; Hu, M.; Zhang, M.; Li, L.; Lv, L.; Li, J. Transcriptome analysis of the innate immunity-related complement system in spleen tissue of *Ctenopharyngodon idella* infected with *Aeromonas hydrophila*. *PLoS ONE* **2016**, *11*, e0157413. [CrossRef]
62. Kishore, U.; Reid, K.B. C1q: Structure, function, and receptors. *Immunopharmacology* **2000**, *49*, 159–170. [CrossRef]
63. Müller-Eberhard, H.J. The membrane attack complex of complement. *Annu. Rev. Immunol.* **1986**, *4*, 503–528. [CrossRef] [PubMed]
64. Barrington, R.; Zhang, M.; Fischer, M.; Carroll, M.C. The role of complement in inflammation and adaptive immunity. *Immunol. Rev.* **2001**, *180*, 5–15. [CrossRef] [PubMed]
65. DeAngelis, R.A.; Markiewski, M.M.; Lambris, J.D. Liver regeneration: A link to inflammation through complement. *Adv. Exp. Med. Biol.* **2006**, *586*, 17–34. [CrossRef] [PubMed]
66. Chen, D.D.; Guo, L.F.; Yi, C.; Wang, S.Q.; Ru, Y.Y.; Wang, H. Hepatopancreatic transcriptome analysis and humoral immune factor assays in red claw crayfish (*Cherax quadricarinatus*) provide insight into innate immunomodulation under *Vibrio parahaemolyticus* infection. *Ecotoxicol. Environ. Saf.* **2021**, *217*, 112266. [CrossRef] [PubMed]
67. Li, M.; Xu, C.J.; Li, D.; Wu, G.F.; Wu, G.Q.; Yang, C.Y.; Pan, Y.F.; Pan, Z.Q.; Tan, G.L.; Liu, Y.Y. Transcriptome analysis of the spleen provides insight into the immunoregulation of *Cyprinus carpio* koi under *Aeromonas veronii* infection. *Aquaculture* **2021**, *540*, 736650. [CrossRef]
68. He, Z.; Chen, X.; Zhao, J.; Hou, D.; Fu, Z.; Zhong, Y.; Hu, X.; Zhang, S.; Sun, C. Establishment of infection mode and *Penaeus monodon* hemocytes transcriptomics analysis under decapod iridescent virus 1 (DIV1) challenge. *Aquaculture* **2021**, *542*, 736816. [CrossRef]
69. Pierce, C.F.; Brown, V.R.; Olsen, S.C.; Boggiatto, P.; Pedersen, K.; Miller, R.S.; Speidel, S.E.; Smyser, T.J. Loci associated with antibody response in feral swine (*Sus scrofa*) infected with *Brucella suis*. *Front. Vet. Sci.* **2020**, *7*, 554674. [CrossRef]
70. Wu, L.T.; Qin, Z.D.; Liu, H.P.; Lin, L.; Ye, J.M.; Li, J. Recent advances on phagocytic B cells in teleost fish. *Front. Immunol.* **2020**, *11*, 824. [CrossRef]
71. Weiss, G.; Schaible, U.E. Macrophage defense mechanisms against intracellular bacteria. *Immunol. Rev.* **2015**, *264*, 182–203. [CrossRef] [PubMed]
72. Savina, A.; Amigorena, S. Phagocytosis and antigen presentation in dendritic cells. *Immunol. Rev.* **2007**, *219*, 143–156. [CrossRef]
73. Kumar, G.; Hummel, K.; Noebauer, K.; Welch, T.J.; Razzazi-Fazeli, E.; El-Matbouli, M. Proteome analysis reveals a role of rainbow trout lymphoid organs during *Yersinia ruckeri* infection process. *Sci. Rep.* **2018**, *8*, 13998. [CrossRef]
74. Blander, J.M. Coupling toll-like receptor signaling with phagocytosis: Potentiation of antigen presentation. *Trends Immunol.* **2007**, *28*, 19–25. [CrossRef] [PubMed]
75. Gilmore, T.D. The Rel/NF-kappaB signal transduction pathway: Introduction. *Oncogene* **1999**, *18*, 6842–6844. [CrossRef] [PubMed]
76. Yoshida, T.; Yamashita, M.; Horimai, C.; Hayashi, M. Smooth muscle-selective inhibition of nuclear factor-κB attenuates smooth muscle phenotypic switching and neointima formation following vascular injury. *J. Am. Heart Assoc.* **2013**, *2*, e000230. [CrossRef]
77. Hayden, M.S.; Ghosh, S. Shared principles in NF-kappaB signaling. *Cell* **2008**, *132*, 344–362. [CrossRef]
78. Lung, H.L.; Kan, R.; Chau, W.Y.; Man, O.Y.; Mak, N.K.; Fong, C.H.; Shuen, W.H.; Tsao, S.W.; Lung, M.L. The anti-tumor function of the IKK inhibitor PS1145 and high levels of p65 and KLF4 are associated with the drug resistance in nasopharyngeal carcinoma cells. *Sci. Rep.* **2019**, *9*, 12064. [CrossRef]
79. Blackwell, T.S.; Christman, J.W. The role of nuclear factor-kappa B in cytokine gene regulation. *Am. J. Respir. Cell Mol. Biol.* **1997**, *17*, 3–9. [CrossRef]
80. Zhou, X.X.; Wang, L.; Feng, H.; Guo, Q.L.; Dai, H.P. Acute phase response in Chinese soft-shelled turtle (*Trionyx sinensis*) with *Aeromonas hydrophila* infection. *Dev. Comp. Immunol.* **2011**, *35*, 441–451. [CrossRef]